Modeling of steady motion and vertical-plane dynamics of a tunnel hull

Christopher S. Chaney and Konstantin I. Matveev

School of Mechanical and Materials Engineering, Washington State University, Pullman, USA

ABSTRACT: *High-speed marine vehicles can take advantage of aerodynamically supported platforms or air wings to increase maximum speed or transportation efficiency. However, this also results in increased complexity of boat dynamics, especially in the presence of waves and wind gusts. In this study, a mathematical model based on the fully unsteady aerodynamic extreme-ground-effect theory and the hydrodynamic added-mass strip theory is applied for simulating vertical-plane motions of a tunnel hull in a disturbed environment, as well as determining its steady states in calm conditions. Calculated responses of the boat to wind gusts and surface waves are demonstrated. The present model can be used as a supplementary method for preliminary estimations of performance of aerodynamically assisted marine craft.*

KEY WORDS: Tunnel hull; Boat dynamics; Ground-effect aerodynamics; Planing surfaces.

INTRODUCTION

Ultra-fast boats and wing-in-ground craft utilize aerodynamic lift to either partially or completely support the vehicle's weight at sufficiently high speeds. This usually results in increased lift-drag ratio. However, such marine vehicles can also become less stable and respond more dramatically to wind gusts and surface waves (Matveev and Kornev, 2013).

The main subject of this paper is the modeling of the vertical-plane dynamics of a tunnel hull (Fig. 1), which is one of the most common configurations of fast boats with aerodynamic unloading. Side planning hulls on this boat remain in contact with water most of the time, whereas the above-water platform generates aerodynamic support. Linear stability of a tunnel hull was analyzed by Kornev et al. (2010). Some aspects of aero-hydrodynamics, stability and dynamics of other aerodynamically assisted marine craft were considered by Nangia (1987), Collu et al. (2010), Gu et al. (2011), and Matveev (2012).
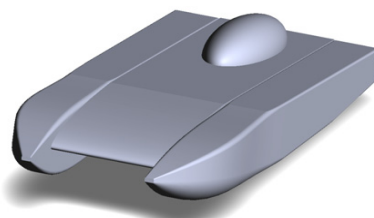

Fig. 1 Three-dimensional render of a simplified tunnel hull.

Corresponding author: *Konstantin I. Matveev*, e-mail: *matveev@wsu.edu*

To calculate aerodynamic lift on a platform moving above but close to the water surface, the extreme-ground-effect theory can be applied (Rozhdestvensky, 2000). Previously, Chaney and Matveev (2012) utilized a steady quasi-one-dimensional formulation of that theory. In this paper, a fully unsteady nonlinear model with transverse variation of airflow and pressure is implemented. The unsteady hydrodynamic forces on planning hulls are determined with the commonly used added-mass strip theory (e.g., Martin, 1978). The next section outlines the mathematical model, and numerical results for a selected configuration are presented in the following section.

Mathematical model

A schematic of a tunnel hull with simplified geometry is given in Fig. 2. Since only vertical-plane motions of this craft at relatively small pitch angles τ are considered here, the vehicle dynamics is governed by the following equations,

$$m\frac{dU}{dt} = T_x - F_D \tag{1}$$

$$m\frac{d^2 y_{cg}}{dt^2} = F_L - mg \tag{2}$$

$$I\frac{d^2 \tau}{dt^2} = M \tag{3}$$

where m and I are the boat mass and moment of inertia, respectively, U is the boat horizontal speed, T_x is the horizontal thrust component, F_D is the total drag force, y_{cg} is the vertical position of the center of gravity, F_L is the total lift force, g is the gravity constant, M is the sum of all moments with respect to the center of gravity (CG), and t is the time.

(a)

(b)   (c)
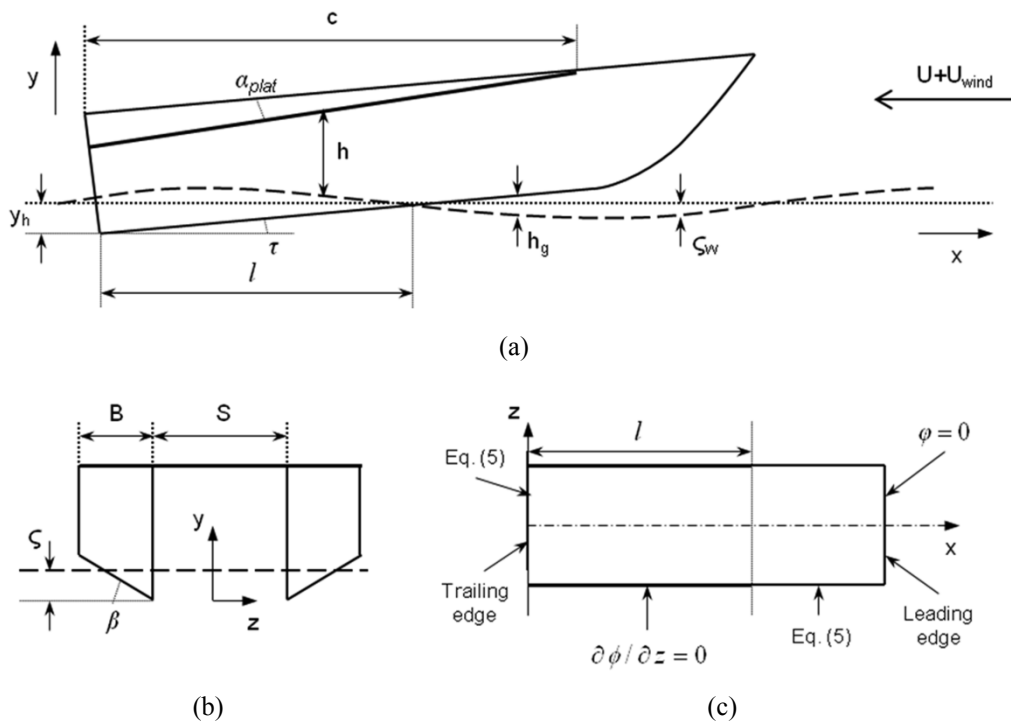
Fig. 2 Tunnel hull schematic views. (a) side view. dashed curve represents water surface.
(b) front view. (c) top view of the platform with boundary conditions for the aerodynamic sub-model.

In the Extreme-Ground-Effect (EGE) theory approximation (Rozhdestvensky, 2000), i.e., when the clearance between the platform and surface is much smaller than the platform length, the aerodynamic lift is predominantly caused by increased pressure underneath the platform. The governing continuity equation for the under-platform quasi-two-dimensional airflow under inviscid and incompressible assumptions is

$$\frac{\partial}{\partial x}\left(h\frac{\partial \phi}{\partial x}\right)+\frac{\partial}{\partial z}\left(h\frac{\partial \phi}{\partial z}\right)=U_{tot}\frac{\partial h}{\partial x}-\frac{\partial h}{\partial t} \tag{4}$$

where φ is the perturbed air velocity potential, axis x is the longitudinal direction, axis z is in the transverse direction, h is the local clearance under the platform, and $U_{tot}=U+U_{wind}$ is the total incident airflow velocity, which can include the wind velocity U_{wind}. In the EGE theory, φ is taken as zero at the platform leading edge, and a zero-gage pressure condition is imposed at the open portion of the side edge,

$$2U_{tot}\frac{\partial \phi}{\partial x}-2\frac{\partial \phi}{\partial t}-\left(\frac{\partial \phi}{\partial x}\right)^2-\left(k\frac{\partial \phi}{\partial z}\right)^2=0 \tag{5}$$

where $k \approx h/(0.61h_g)$ accounts for sidewise air leakage (including jet contraction) under the side hull with gap h_g (Fig. 2). A similar boundary condition but with $k=1$ is applied at the trailing edge. Along the closed part of the side platform, where the lateral flow is absent, $\partial \phi/\partial z=0$.

The velocity potential φ is calculated numerically with an implicit second-order finite difference method using information for the vehicle geometry and position, values of φ from the previous time step, the water surface elevations, and the wind speed. The numerical cell dimensions Δx and Δz are selected as 1/28 of the platform length and 1/12 of the platform beam, respectively. The time step is chosen as $\Delta t = \Delta x/(2U)$. Smaller time steps or finer mesh are found not to lead to significant changes in results. At each time step, an iterative solution procedure is employed since Eq. (5) is nonlinear. After determining φ, the gage pressure under the platform due to partially-stagnated airflow is computed with the unsteady Bernoulli equation,

$$p_g = \rho_a\left[U_{tot}\frac{\partial \phi}{\partial x}-\frac{\partial \phi}{\partial t}-\frac{1}{2}\left(\frac{\partial \phi}{\partial x}\right)^2-\frac{1}{2}\left(\frac{\partial \phi}{\partial z}\right)^2\right] \tag{6}$$

where ρ_a is the air density.

The instantaneous platform lift F_{Lp} and lift-induced drag F_{Dp} due to higher pressure under the platform, as well as the center of aerodynamic lift, can be found by integrating the gage pressure over the platform area S under the assumption of small trim angles of the platform,

$$F_{Lp} \approx \int_S p_g\,dS \tag{7}$$

$$F_{Dp} \approx \int_S p_g\frac{dh}{dx}\,dS \tag{8}$$

$$X_{Lp} \approx \frac{1}{F_{Lp}}\int_S xp_g\,dS \tag{9}$$

The aerodynamic extreme-ground-effect theory is relatively new and only a few validation cases can be found in the literature (Rozhdestvensky, 2000; Soderlund and Matveev, 2010). Here, a comparison with another experiment is demonstrated. Gallington and Miller (1970) carried out wind tunnel tests with a ground-effect platform, depicted in Fig. 3(a). The model had side plates and a trailing-edge interceptor (short vertical plate). The experimentally measured pressure coefficient, $C_p = p_g /(0.5\rho_a U^2)$, is compared in Fig. 3(b) with values calculated by the method outlined above. A reasonably good agreement is observed. A relatively small deviation between test data and numerical results can be caused by viscous effects that are usually pronounced in small-scale model tests.
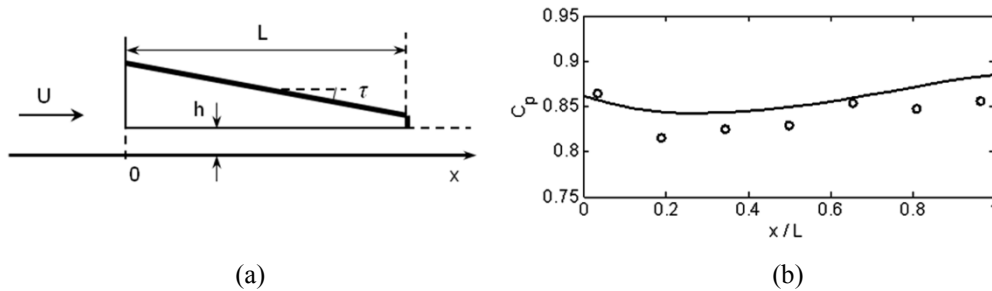

Fig. 3 (a) Schematic of an experimental ground-effect platform model. (b) distribution of pressure coefficient along the model centerline. circles, test data; curve, results of the present method.

Hydrodynamic forces on the planing hulls are determined with the standard added-mass strip theory (Martin, 1978). The hulls are divided into a number of transverse sections, and a local hydrodynamic force exerted normally to the hull surface is found from a local change of the water flow momentum. The total force is then determined by integrating over the wetted keel length l,

$$F_{AM} = \int_0^l \frac{d}{dt}(\mu\dot{\varsigma})\,dx \tag{10}$$

where μ is the added mass of the local hull section, and $\dot{\varsigma}$ is the component of the relative water velocity normal to the keel. The added masses for single-deadrise hulls (Fig. 2) and additional cross-flow and buoyancy-suction corrections applied in this study are taken from Martin (1978) and Payne (1988). In particularly, the two-dimensional added mass equals to

$$\mu = C_m \rho_w \pi \left(\frac{b'}{2}\right)^2 \tag{11}$$

where ρ_w is the water density, b' is the wetted beam of the hull section, and coefficient C_m is calculated from the empirical correlations,

$$C_{m,1} = C_0 = \frac{1}{2}\left(1 - \frac{\beta}{\pi} + \sqrt{\frac{\sin\beta}{5}}\right) \tag{12}$$

$$C_{m,2} = C_0 + \frac{2}{3}\left(\frac{\varsigma}{b} - \tan\beta\right) \tag{13}$$

where β is the hull deadrise angle, b the hull beam, and ς is the keel submergence of the considered hull section. Eqs. (12) and (13) are applied for the dry-chine and wet-chine sections, respectively.

The water velocity normal to the hull that appears in Eq. (10) is determined via equation suggested by Martin (1978) under the assumption of small trim angles,

$$\dot{\varsigma} = \tau U - \dot{y}_h - \dot{\tau}(x - x_h) + \dot{\varsigma}_w \tag{14}$$

where y_h and x_h are the coordinates of the hull transom edge and $\dot{\varsigma}_w$ is the wave-induced water velocity. For low-amplitude regular waves in the head or following directions, the wave component is

$$\dot{\varsigma}_w = \mp A_w \omega \sin[k_w(x + s \pm c_w t)] \tag{15}$$

where A_w is the wave amplitude, $\omega = c_w k_w$ is the wave angular frequency, $c_w = \sqrt{g/k_w}$ is the wave propagation velocity, g is the gravity, $k = 2\pi/\lambda$ is the wave number, λ is the wavelength, and $s = \int_0^t U dt$ is the distance traveled by the boat. The upper signs on the right-hand side of Eq. (15) are for the head waves, whereas the lower signs correspond to the following waves.

The added-mass theory has been previously validated for a variety of planing hulls (e.g., Martin, 1978; Payne, 1988). However, a combination of this theory with the aerodynamic model employed in this study has not been validated yet due to absence of complete experimental information for aerodynamically assisted boats in the open literature.

The propulsor thrust force is assumed to be parallel to the hull keel line. Additional drag force components, including hydrodynamic drag of appendages, friction drag on the wetted hull surface and aerodynamic drag of the boat superstructure, are modeled in a simplified form,

$$F_d = C_d \frac{\rho u^2}{2} A \tag{16}$$

where C_d and A are the appropriate empirical drag coefficient and reference area, and ρ and u are the fluid density and velocity of the incident flow.

With given expressions for all forces, the governing dynamics equations (Eqs. (1)-(3)) can be integrated in time to predict the boat vertical-plane motions. The computational model hierarchy is schematically depicted in Fig. 4.
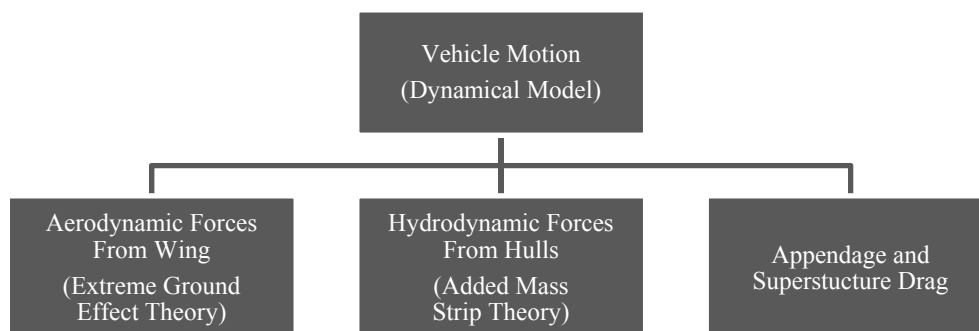

Fig. 4 Block-diagram of numerical models.

RESULTS AND DISCUSSION

The configuration of the boat modeled in this paper is selected to resemble off-shore racing tunnel hulls. Simplified geometry is chosen to avoid unnecessary complexity in modeling and result presentation. Side hulls have single deadrise, as is typically used in such boats to reduce spray in the tunnel. Hull cross-sections are uniform and do not incorporate steps. The platform has a chord of 10*m* and a span of 1.5*m* with an aspect ratio of 0.15. The platform is set 0.4*m* above the hull transom and inclined at a 2.5° incidence with respect to the keel. Vehicle geometry is given in Table 1. Superstructure and appendage information is also included in Table 1 for evaluating additional drag via Eq. (16).

Table 1 Main parameters of the considered tunnel hull.

Platform span	S	1.5m
Horizontal station of CG	X_{cg}	2m
Platform chord	c	10m
Vehicle mass	M	5000kg
Trailing edge height off keel	Y_{pl}	0.4m
Angle of platform off keel	α_{plat}	2.5°
Individual hull beam	B	1m
Hull deadrise	β	12°
Chine height	H_c	0.21m
Vertical station of CG	Y_{cg}	0.5m
Superstructure height	S_h	1m
Superstructure drag coefficient	C_{dsup}	0.2
Appendage area	A_{app}	0.025m^2
Appendage drag coefficient	C_{dapp}	0.1

One of the novelties of this paper is the implementation of EGE theory for finding aerodynamic lift on the platform. Sample calculated pressure distributions are shown in Fig. 5. These results correspond to the geometry of the tunnel hull boat operating in a characteristic condition with completely sealed side plates (Fig. 5(a)), completely open side plates (Fig. 5(b)), and partly open sides (Fig 5(c)). For the partially sealed case, the aft 1.6-m hull sections are submerged and the foremost 8.4m of the platform experiences lateral air leakage under the hulls. This characteristic condition is defined at 17kN of thrust, corresponding to a vehicle forward speed of 68m/s, and a platform trim angle of 5.2°.

The completely sealed condition, shown in Fig. 5(a), displays the anticipated 2D pressure distribution. With no lateral flow allowed, velocity and pressure vary only along x. For this condition, the trailing edge gap is sufficiently small to cause significant air stagnation and high pressure in the front part of the platform. Fig. 5(b) shows the pressure distribution under the platform for the case of no side hulls. Unimpeded lateral air flow results in small pressure recovery under the platform. The gage pressure is much smaller than in the case of sealed sides. A typical pressure distribution with partially restricted sides is depicted in Fig. 5(c). The most pressure is recovered at the sections where the hulls intersect the water surface.
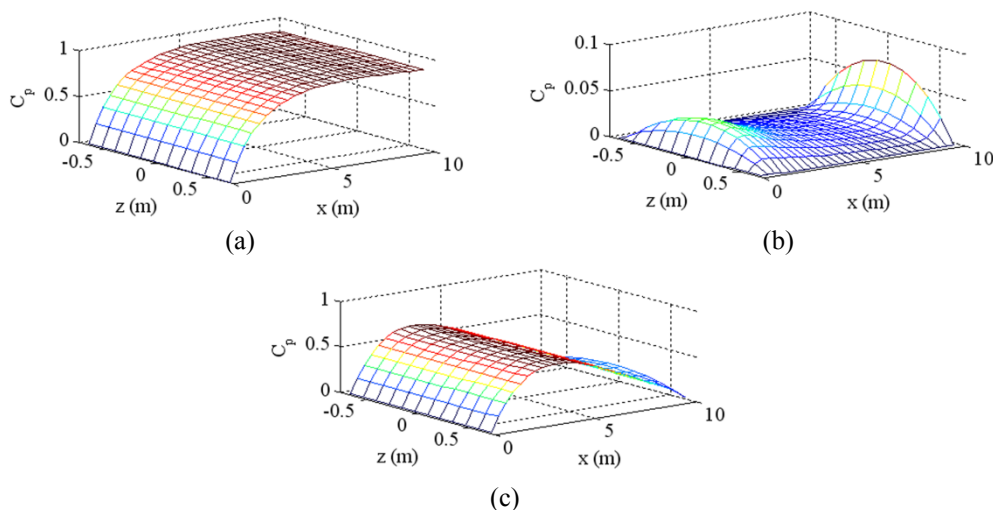

Fig. 5 Two-dimensional steady pressure distributions for the tunnel hull platform.
(a) sealed sides, (b) no side plates, (c) partially sealed sides.

Calculations have been performed to determine equilibrium states for the specified tunnel hull boat. The required thrust, T, center of gravity height with respect to the water surface, h_{cg}, keel trim angle, α, and the ratio of aerodynamic lift to total lift are expressed as functions of the equilibrium forward speed, U, and shown in Fig. 6. Fig. 6(a) depicts the thrust required to maintain a certain velocity. Unsurprisingly, increasing vehicle velocity requires increased thrust. The slope of the thrust-velocity relation is somewhat nonlinear, and exhibits larger slopes at the extremes of the analyzed range. At low speeds, hydrodynamic lift dominates, resulting in large hydrodynamic drag, which produces the large slope in this region. As velocity increases, aerodynamic lift becomes more important (Fig. 6(d)). The aerodynamic lift produces less drag per unit lift than the hydrodynamic lift, which reduces the slope. A reasonably efficient point is experienced near 17kN of thrust, which is taken as the characteristic condition for most other simulations in this paper. As the vehicle increases speed further, the appendage and superstructure drag, which are of relatively small at low speeds, start to become a dominant factor. This results in the increased slope at higher speeds.
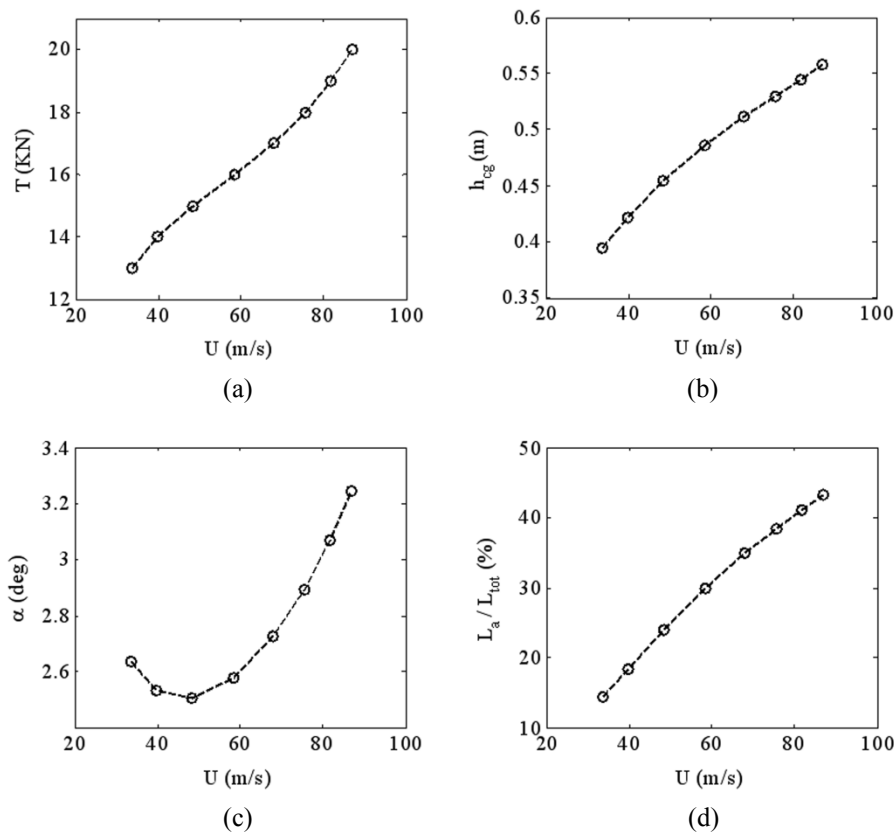

Fig. 6 Equilibrium states of the boat at various forward speeds. (a) required thrust,
(b) CG height, (c) keel trim angle, (d) fraction of aerodynamic lift.

Fig. 6(b) shows the CG height variation with speed. Equilibrium ride height increases with forward velocity. The change of the keel trim angle is illustrated in Fig. 6(c). This relation has a strong curvature, with high trim angles at either extreme. At low velocities, high trim angles are required to maintain sufficient lift to remain afloat. Trim angle initially decreases with forward speed, until the aerodynamic lift starts to become substantial at around 50m/s. The aerodynamic center of pressure on the platform is significantly further forward than the hydrodynamic center of lift on the hulls, resulting in increased pitch at higher speeds.

Fig. 6(d) illustrates the aerodynamic lift as a percent of the total lift. In equilibrium, the vehicle total lift always equals to its weight, therefore, this figure can be also used to quantify the ratio between aerodynamic and hydrodynamic lift components. At the highest speeds studied, the aerodynamic lift supports nearly half of the boat weight. Higher velocities are possible with sufficient thrust; however, the equilibrium pitch angle of the platform starts to become too large for the mathematical model to remain valid.

Time-domain simulations have been conducted for the tunnel hull boat moving under the influence of wind gusts. The vehicle's response in velocity, trim, and CG height to both head and following gusts is shown in Fig. 7. The simulations start from an equilibrium state corresponding to thrust level of 20*kN*; and a stepped wind perturbation is imposed with duration of six seconds. Vehicle responses can be broken into three distinct regimes: initial equilibrium motion, transient motions during the wind gust, and attenuating motions back to equilibrium after the gust.
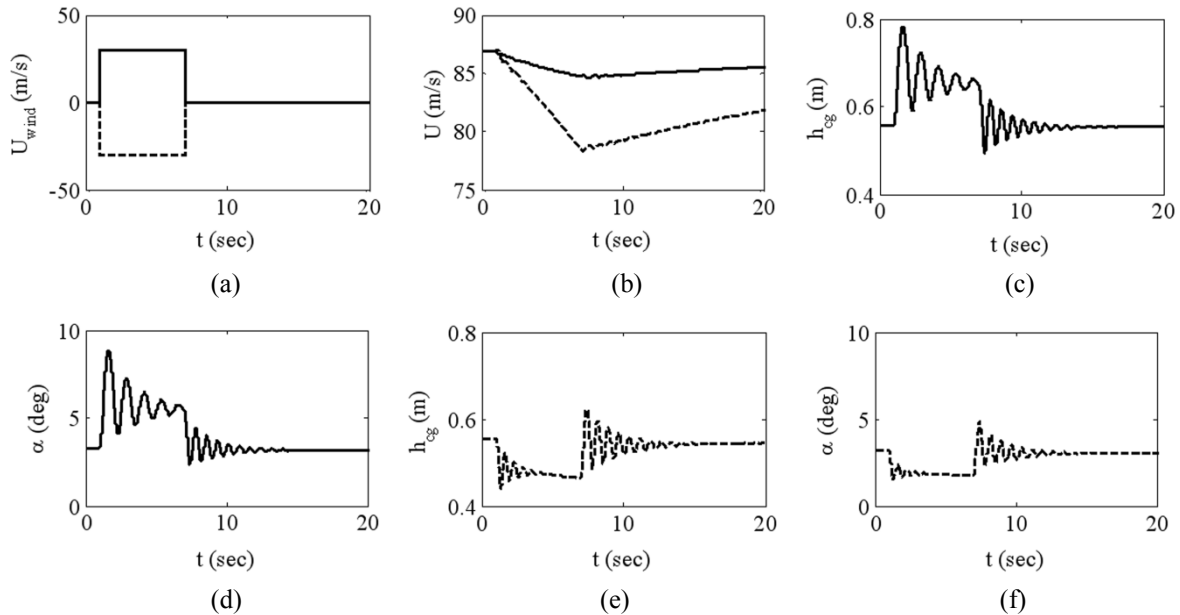

Fig. 7 Boat response to wind gusts. (a) Wind gust velocity, (b) boat forward speed, (c) and (e) CG height, (d) and (f) pitch angle. Solid lines, head gust; dotted lines, following gust.

The vehicle forward velocity decreases in response to both head and following wind gusts for the given equilibrium state (Fig. 7(b)); however this trend can change if the boat is perturbed from other equilibriums. The head gust increases aerodynamic lift which reduces lift-induced drag. However, this reduction is outweighed by the increase of superstructure drag. Very small surge oscillations are experienced during return to equilibrium. Time required for the boat speed to return to equilibrium is much longer than characteristic motions of heave and pitch. For the following wind gust, the reduction in superstructure drag is outweighed by the increase of hydrodynamic drag due to deeper hull submergence (Fig. 7(e)).

As seen in Figs. 7(c) and (d), the boat CG height and trim angle both increase in response to a head gust. Higher aerodynamic lift due to the wind gust decreases the required hydrodynamic lift. Additionally, the location of the aerodynamic center of pressure forward of the hydrodynamic center of lift results in an increased trim angle in response.

Figs. 7(e) and (f) show the vehicle response in CG height and pitch to a following wind gust. Opposite of the head gust, the following gust reduces both center of gravity height and trim angle. Reduced aerodynamic lift causes the vehicle to settle into the water, and increased hydrodynamic lift shifts the total center of lift backward, resulting in a more nose-down attitude. Like the head gust case, the following gust also produces attenuating oscillations in pitch and heave after the application and stop of the wind.

Another dynamic regime of interest is the boat response to water waves. A study is performed to show heave and pitch motions in response to head waves of both 2*cm* and 15*cm* amplitudes with a vehicle thrust of 17*kN*. Height and slope of a 35-*m* long wave at the vehicle CG section are displayed in Figs. 8(a) and (b). The vehicle's response in heave and pitch are presented in Fig. 8(c), (d) for 2-*cm* waves and in Fig. 8(e), (f) for 15-*cm* waves.

The boat exhibits nearly linear behavior for the 2-*cm* wave case shown (Fig. 8(c), (d)). The small-amplitude wave induces a nearly sinusoidal response in heave and pitch at the frequency of encounter. For this wavelength, the CG heave response is slightly out of phase of the wave, with minima and maxima occurring about a quarter period after the peaks and troughs of the wave, respectively. A similar result in pitch is observed, in that the minima and maxima of the pitch angle response lag the wave slope by approximately one quarter of a period.
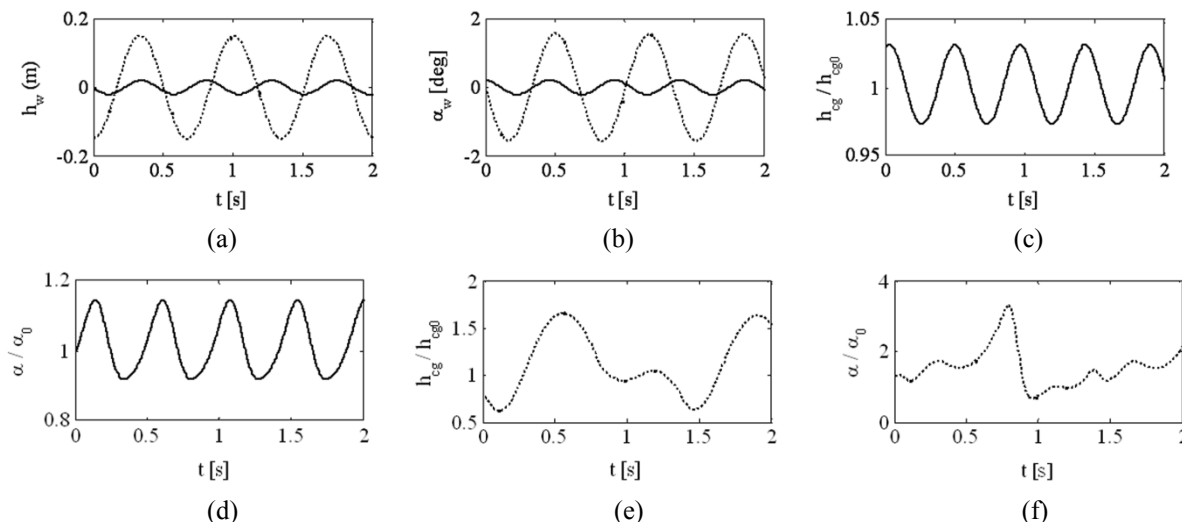
Fig. 8 Vehicle responses to regular waves. (a) wave height at CG, (b) wave slope at CG, (c),
(e) normalized CG height, (d), (f) normalized trim angle. solid lines, 2-*cm* waves; dotted lines,
15-*cm* waves. values with subscript 0 correspond to equilibrium states with no waves.

Very different results are demonstrated in Figs. 8(e) and (f) for the case of the 15-*cm* amplitude wave. The large wave amplitude causes the vehicle to breach from the water once every two cycles. This behavior is highly-dependent on the frequency of the wave and its proximity to resonance. Breaching results in strongly nonlinear boat motion, and heave and pitch response does not resemble the forcing waveform. Breaching occurs approximately one eighth of a period before the trough of every other wave. This event is followed by one period of recovery over which the boat exhibits less extreme motion, and is then repeated. Additionally, both CG heights and trim angles experience higher time-averaged values than the equilibrium state with no waves, h_{cg0} and α_0.

Simulations have been also performed on the boat to study its motions in a range of wavelengths. The boat thrust is fixed at 17kN. Fig. 9 depicts the relative amplitude response to a 2-*cm* amplitude head wave for various wavelength-to-vessel-length ratios. These data show that resonance for both heave and pitch occur near the relative wavelengths of 4.6 ($\lambda = 55m$). For high frequency waves, the relative amplitudes approach zero, as the inertia of the vehicle is too great to respond to the waves. Long wavelengths result in relative amplitudes approaching one, as the wavelengths become so large the vessel operates in a quasi-steady state.
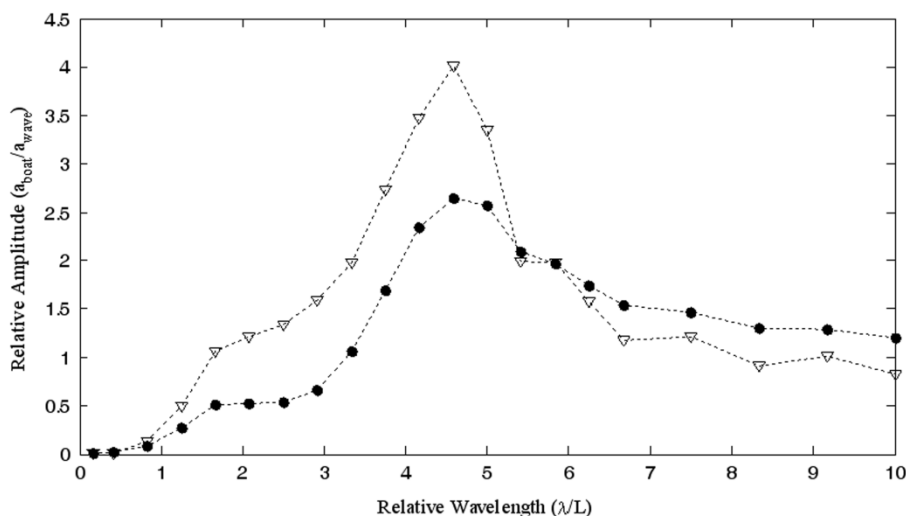

Fig. 9 Amplitudes of boat motions in low-amplitude waves.
solid circles, heave at CG; hollow triangles, pitch angles.

CONCLUDING REMARKS

A simplified mathematical model developed in this work can be used for producing quick simulations of vertical-plane dynamics of tunnel hull boats in wind gusts and waves, as well as for determining their equilibrium states in calm conditions. When fully validated, the current method can be applied for design optimization of marine craft with aerodynamically supported surfaces operating in pronounced ground effect. Results presented in this study illustrate calculated vertical-plane responses of a selected boat configuration to head or following wind gusts and regular waves, acting separately. Since wind gusts and waves are often present simultaneously, the current method can be also used in the future to identify dangerous regimes in such conditions and suggest operational actions for reducing extreme motions and loads on aerodynamically un-loaded boats.

Future development of the mathematical model can include more degrees of freedom, addition of control surfaces, and large-amplitude motions that may possibly lead to accidents, such as boat flipping and slamming. Application of Computational Fluid Dynamics (CFD) methods can improve accuracy of the model's components, although complete unsteady CFD simulations for an entire air-assisted boat would be very costly, especially in a broad range of system conditions. While the present model's expressions for the different forces have been previously validated, experimental validation of the combined dynamic model for a tunnel hull requires complete test information for boats of this type, which is currently unavailable in the open literature. Hence, the applicability of the present method for design of actual boats is rather limited. Calculation results obtained with this model will need further experimental verification.

ACKNOWLEDGEMENT

REFERENCES

Chaney, C.S. and Matveev, K.I., 2012. Modeling of vertical-plane motions of a tunnel hull boat. *Proceedings of the 3rd Chesapeake Power Boat Symposium*, Annapolis, MD, USA, 15-16 June 2012, pp.1-10.

Collu, M., Patel, M. and Trariex, F., 2010. The longitudinal stability of an aerodynamically alleviated marine vehicle. a mathematical model. *Proceedings of the Royal Society A*, 466, pp.1055-1075.

Gallington, R.W. and Miller, M.K., 1970. The ram-wing: a comparison of simple one-dimensional theory with wind tunnel and free flight results. *Proceedings of AIAA Guidance, Control and Fluid Mechanics Conference*, Santa Barbara, CA, 17-19 August 1970, pp.1-9.

Gu, P., Gundersen, R., Kalvik, A.O., Salvesen, R., Karimi, H.R. and Ottestad, M., 2011. Data gathering and mathematical modeling for pitch stabilization of a high speed catamaran. *Modeling, Identification, and Control*, 14(3), pp.149-158.

Kornev, N.V., Kleinsorge, L. and Migeotte, G., 2010. Dynamics and stability of racing boats with air wings. *International Journal of Aerodynamics*, 1, pp.28-51.

Martin, M., 1978. Theoretical determination of porpoising instability of high-speed planing boats. *Journal of Ship Research*, 22(1), pp.32-53.

Matveev, K.I., 2012. Modeling of longitudinal motions of a hydroplane boat. *Ocean Engineering*, 42, pp.1-6.

Matveev, K.I. and Kornev, N., 2013. Dynamics and stability of boats with aerodynamic support. *Journal of Ship Production and Design*, 29(1), pp.17-24.

Nangia, R.K., 1987. Aerodynamic and hydrodynamic aspects of high-speed water surface craft. *The Aeronautical Journal of the Royal Aeronautical Society*, 91(906), pp.241-268.

Payne, P.R., 1988. *Design of High-Speed Boats: Planing*. Annapolis. MD: Fishergate, Inc.

Rozhdestvensky, K.V., 2000. *Aerodynamics of a lifting system in extreme ground effect*. Heidelberg, Germany: Springer-Verlag.

Soderlund, R.K. and Kornev, K.I., 2010. Jet-induced pressure distribution under platform in ground effect. *International Journal of Vehicle Design*, 53(3), pp.133-148.